

Article

An Investigation of Left Ventricular Valve Disorders and the Mechano-Electric Feedback Using a Synergistic Lumped Parameter Cardiovascular Numerical Model

Nicholas Pearce  and Eun-jin Kim 

Center for Fluids and Complex Systems (FSC), Faculty of Engineering, Environment and Computing, Coventry University, Coventry CV1 5FB, UK

* Correspondence: pearcen5@uni.coventry.ac.uk

Abstract: Cardiac diseases and failure make up one of largest contributions to global mortality and significantly detriment the quality of life for millions of others. Disorders in the valves of the left ventricle are a prominent example of heart disease, with prolapse, regurgitation, and stenoses—the three main valve disorders. It is widely known that mitral valve prolapse increases the susceptibility to cardiac arrhythmia. Here, we investigate stenoses and regurgitation of the mitral and aortic valves in the left ventricle using a synergistic low-order numerical model. The model synergy derives from the incorporation of the mechanical, chemical, and electrical elements. As an alternative framework to the time-varying elastance (TVE) method, it allows feedback mechanisms at work in the heart to be considered. The TVE model imposes the ventricular pressure–volume relationship using a periodic function rather than calculating it consistently. Using our synergistic approach, the effects of valve disorders on the mechano-electric-feedback (MEF) are investigated. The MEF is the influence of cellular mechanics on the electrical activity, and significantly contributes to the generation of arrhythmia. We further investigate stenoses and regurgitation of the mitral and aortic valves and their relationship with the MEF and generation of arrhythmia. Mitral valve stenosis is found to increase the sensitivity to arrhythmia-stimulating systolic stretch, and reduces the sensitivity to diastolic stretch. Aortic valve stenosis does not change the sensitivity to arrhythmia-stimulating stretch, and regurgitation reduces it. A key result is found when valve regurgitation is accompanied by diastolic stretch. In the presence of MEF disorder, ectopic beats become far more frequent when accompanied by valve regurgitation. Therefore, arrhythmia resulting from a disorder in the MEF will be more severe when valve regurgitation is present.

Keywords: non-linear dynamics; multiscale model; cardiac cycle; mechano-electric feedback; lumped-parameter model



Citation: Pearce, N.; Kim, E.-j. An Investigation of Left Ventricular Valve Disorders and the Mechano-Electric Feedback Using a Synergistic Lumped Parameter Cardiovascular Numerical Model. *Bioengineering* **2022**, *9*, 454. <https://doi.org/10.3390/bioengineering9090454>

Academic Editors: Alexander V. Panfilov and Bum-Rak Choi

Received: 5 June 2022

Accepted: 5 September 2022

Published: 8 September 2022

Publisher's Note: MDPI stays neutral with regard to jurisdictional claims in published maps and institutional affiliations.



Copyright: © 2022 by the authors. Licensee MDPI, Basel, Switzerland. This article is an open access article distributed under the terms and conditions of the Creative Commons Attribution (CC BY) license (<https://creativecommons.org/licenses/by/4.0/>).

1. Introduction

Out of the many cardiovascular diseases plaguing millions of people throughout the world, disorders in the heart's valves make up a significant proportion. These disorders frequently lead to death or morbidity, particularly in the ageing population [1]. Disorders in the left ventricle valves are more numerous than those in the right ventricle, with disease in the aortic valve making up the largest proportion of valvular deaths [2]. The three main disorders affecting the heart valves are prolapse, stenosis and regurgitation. Further, these pathologies can increase susceptibility to arrhythmia in the atrium and whole heart. It is known, for example that mitral valve prolapse may excite the electrical dynamics of the heart leading to cardiac arrhythmia [3]. This is thought to be caused by the increased stretching of the valve leaflets during systole, which in turn excites the electrical messaging in the ventricle via a mechanism called the mechano-electric feedback (MEF) [4]. Additional to the resulting arrhythmia, sudden cardiac death may also occur [3]. Valve prolapse may also cause regurgitation, which increases myocardial load and hence, stretching of the

cardiac muscles [5]. Studies of valve patients that have recovered from arrhythmia as a complication frequently find fibrosis in the left-ventricular wall; evidence of excessive stretch [6]. Mitral valve stenosis is often associated with arrhythmia and is due to the excessive stretching of the left atrium [7].

Despite the heart's apparent complexity, it remains a well-regulated organ and this is aided by many feedback mechanisms at work over multiple scales and domains; from the micro cellular scale of the myocytes to the macro organ level scale. The MEF is one of the main feedback mechanisms. Along with the electro-excitation coupling (ECC), these two mechanisms help maintain cardiac stability and synchronicity. As their names suggest, the MEF is the feedback of local mechanical cell stretch on the electrical dynamics, while the ECC operates in the opposite direction. For comprehensive reviews of the MEF see [8,9]. Whilst the MEF helps maintain synchronicity, it can have some peculiar consequences, particularly in the generation and termination of arrhythmia. Commitio-cordis, which is the mortal induction of fibrillation by an innocent impact to the chest is perhaps the most peculiar. Link et al. [10,11] conducted an illustrative set of clinical experiments studying how ventricular mechanical stretch can excite the cardiac electrical activity and induce arrhythmia. This is found to be highly dependent on the ECG timing, with only those cases in which stretching occurred during a certain window of the ECG initiating arrhythmia. A review of the recent clinical studies into mechanically induced electrophysiological behaviour is provided in [5]. Stretch-activated-channels (SACs) are the leading mechanism thought to be responsible for the MEF [9,12], though other mechanisms may also be involved. SACs are cells which open or close cellular ion channels in response to mechanical stretch and for the left ventricle, their response depends on the timing during the cardiac cycle [10,13,14]. Stimulating these channels can thereby change the character of the action potential: the electrical wave that causes cell contraction and relaxation. The action potential changes depend on the period in the cardiac cycle at which stretch is induced.

Computer and mathematical modelling is a powerful way to investigate complex systems as it allows for system visualisation, hypotheses and predictions to be examined at relatively low cost compared to experimental methods [15]. Computer models of the cardiovascular system vary in complexity, from simple zero dimensional (0D) and one dimensional (1D) models to full three dimensional (3D) models, some involving motion of structure. Numerical investigations of the heart valves likewise vary in complexity. 0D and 1D models involving the heart valves frequently use a 'diode' approach in which the dynamics of the valve are ignored and the direction of flow imposed similar to an electrical diode [16,17], while fully 3D examples most frequently use stiff geometry and studies using dynamic values [18] are rare. The 3D structural models provide flow field information and include interaction between the tissue structure and flow [18–20]. Complex numerical models involving cellular mechanics, electrophysiology, ion movements, and 3D models requiring detailed mathematical solution do not lend themselves to the demanding clinical environment due to their high cost in terms of computational load and time [21]. Numerical models of MEF likewise vary in complexity, with plenty of examples of relatively simple low-order 0D and 1D studies [12,22–24] and full cardiovascular system and 3D models [25–27].

In this study a 0D mathematical model of the left ventricle with valve stenoses and regurgitation is developed, by modifying the synergistic cardiovascular model by Kim and Capoccia [28]. The model consistently simulates the coupling of the mechanical, chemical and electrical functions of the myofiber on the micro-scale as well as the macro-scale organ activity. The consideration of different domains and scales gives it a synergistic quality, which is similar to Roy et al. [16] who control organ dynamics through the electrophysiology. Their haemodynamic activity is controlled using the time-varying-elastance (TVE) method however, in which the ventricular pressure–volume relationship is imposed using a periodic function [29,30] instead of calculating it consistently. The TVE paradigm has frequently been questioned [17,31] when used for cardiovascular modelling due to its empirical foundations

and neglect of haemodynamic-regulating feedback mechanisms. Use of the adopted model [28] bypasses the need to use the TVE method due to its synergistic approach. The model has been validated as an alternative to the TVE method [28] and previously used for the study of dilated cardiomyopathy, left ventricular assist devices (LVADs) and MEF [32,33]. In [32], the model proved capable at reproducing known MEF effects consistent with previous findings by others, for example a prolonged action potential duration consistent with [34], and ectopic peaks in electrical patterns along with rapid oscillation consistent with the effect of SACs seen in [9,27,35]. The rest of the paper is organised as follows: the cardiovascular system model is described in Section 2; in Section 3, the results of using the model to simulate valve and MEF pathologies are described; in Section 4, these results are discussed; and in Section 5 a conclusion to this study is provided.

2. Materials and Methods

The cardiovascular system model is made of three parts presented in Sections 2.1–2.4 as follows. First, in Section 2.1, the micro-scale sarcomere model is described. This is followed in Section 2.2, by the macro, organ scale dynamics model. The electro-chemical activity model is described in Sections 2.3 and 2.4 describes the method for simulating valve pathologies. Table 1 gives the physiological meaning of the model variables. Tables 2 and 3 provide the meaning and values of the model parameters used for a control case representing a ‘healthy’ pathology-free heart.

Table 1. Variables and their physiological meaning.

Variable	Physiological Description
v_c	Velocity of the contractile element (s^{-1})
ϵ_c	Strain of the contractile element
τ_c	Active tension of the contractile element (mmHg)
k_c	Stiffness of the contractile element (mmHg)
σ_p	Passive stress (mmHg)
u	Chemical activity (s^{-1})
p	Slow electric variable
q	Fast electric variable
P_v	Left ventricular pressure (mmHg)
P_r	Left atrial pressure (mmHg)
P_s	Systemic pressure (mmHg)
m	Aortic pressure (mmHg)
F_a	Aortic flow (mL/s)

Table 2. Control parameters for ventricle micro-scale mechanical and electrical models.

Parameter	Value	Physiological Description
σ_0	240 kPa	Maximum left ventricle sarcomere active tension
k_0	120 kPa	Maximum left ventricle sarcomere active elastance
k_1 ,	0.002 kPa	Passive tension parameter
k_2	14 kPa	Passive tension parameter
χ, α_1	$100 s^{-1}, 10 m^{-1}$	Damping parameters
ω_0	$100 s^{-1}$	Microscale oscillation frequency
a, b	$100 m s^{-2} kPa^{-1}, 6000 m s^{-2}$	Active and passive tension parameter
β_0	$\frac{40}{3.5} mL^{-2}$	Frank-starling length-tension parameter
γ	0.6	Left ventricle pressure parameter
V_0	$\frac{144}{1.5} mL$	Left ventricle volume parameter
α_u	$5 s^{-1}$	Ventricle sarcomere chemical excitation parameter
μ_1, μ_2	$0.0024 kPa^{-1}, 0 (s mL)^{-1}$	Ventricle MEF parameters

Table 3. Circulation parameters.

Parameter	Value	Physiological Description
R_a	0.001 mmHg s/mL	Aortic valve resistance
R_m	0.005 mmHg s/mL	Mitral valve resistance
R_c	0.0398 mmHg s/mL	Characteristic resistance
R_s	0.5 mmHg s/mL	Systemic resistance
C_s	1.33 mL/mmHg	Systemic compliance
C_a	0.08 mL/mmHg	Aortic compliance
C_r	4.4 mL/mmHg	Atrial compliance
L_s	0.0005 mmHg s ² /mL	Inertance of blood in aorta

2.1. Micro-Scale Model

The micro-scale mechanical model by Kim and Capoccia [28] is based on the Bestel–Clement–Sorine (BCS) formulation [36,37] for myofiber dynamics. It is derived from the Hill–Maxwell rheological model of a myofiber in which the active contractile sarcomere is placed in series with another elastic element that simulates the active relaxation. These two elements are surrounded by connective tissues which is modelled by a third elastic element in parallel to the active and passive sarcomere parts. This parallel element stops the heart exceeding its limits [38]. The governing equations below describe the velocity $v_c = \frac{d\epsilon_c}{dt}$, strain ϵ_c , stress τ_c , and stiffness k_c of the active contractile element, represented by the subscript ‘c’. Equation (5) below for $d_0(\epsilon_c)$ represents the Frank-Starling law for cell stretch.

$$\frac{dv_c}{dt} = -\chi\tau_c - \omega_0^2\epsilon_c - a\tau_c d_0(\epsilon_c) + b\left(\sqrt{\frac{V}{V_0}} - 1\right), \tag{1}$$

$$\frac{d\epsilon_c}{dt} = v_c, \tag{2}$$

$$\frac{d\tau_c}{dt} = k_c v_c - (a_1|v_c| + |u|)\tau_c + \sigma_0 u_+, \tag{3}$$

$$\frac{dk_c}{dt} = -(a_1|v_c| + |u|)k_c + k_0 u_+, \tag{4}$$

$$d_0(\epsilon) = e^{-\beta_0(\epsilon_c - 0.1)^2}. \tag{5}$$

Here, the ‘+’ subscript means that only positive values of the preceding term are included, otherwise the term is 0. The first term $\chi\tau_c$ in Equation (1) represents a damping force, $\omega_0^2\epsilon_c$ represents a harmonic force, $a\tau_c d_0(\epsilon_c)$ is an active force, and $b\left(\sqrt{\frac{V}{V_0}} - 1\right)$ is a passive force. u simulates the calcium bound Troponin-C concentration responsible for cell activation. The last term in Equations (3) and (4) represents the activation of the contractile force, while the term $(a_1|v_c| + |u|)$ models the deactivation. σ_0 and k_0 are constants representing the maximum cell stress and stiffness, respectively. The parallel stress element in the Hill–Maxwell model is represented here by σ_p and evolves exponentially according to Equation (6) below.

$$\sigma_p = \frac{k_2}{k_1} [\exp(k_1 \sqrt{V/V_0}) - 1], \tag{6}$$

in which k_1 and k_2 are constants for passive tension.

2.2. Macroscale Model

The micro-scale part of the model is coupled to the macro organ scale part through the left ventricle pressure P_v according to Equation (7) below.

$$P_v = \gamma \frac{V_0}{V} [d_0(\epsilon_c)\tau_c + \sigma_p]. \tag{7}$$

γ in Equation (7) is a constant representing the ventricular wall thickness to radius ratio. The ventricle volume V and circulation models evolve according to Equations (8)–(12) below, in which m is the aortic pressure, F_a is the aortic flow, P_r is the left atrial pressure, and P_s is the systemic pressure.

$$\frac{dV}{dt} = \frac{U_{mi}(P_r - P_v)}{R_m} - \frac{U_{ao}(P_v - m)}{R_a}, \tag{8}$$

$$\frac{dm}{dt} = -\frac{F_a}{C_a} + \frac{U_{ao}(P_v - m)}{C_a R_a}, \tag{9}$$

$$\frac{dF_a}{dt} = \frac{m - P_s}{L_s} - \frac{R_c F_a}{L_s}, \tag{10}$$

$$\frac{dP_r}{dt} = \frac{P_s - P_r}{C_r R_s} - \frac{U_{mi}(P_r - P_v)}{C_r R_m}, \tag{11}$$

$$\frac{dP_s}{dt} = \frac{P_r - P_s}{C_s R_s} + \frac{F_a}{C_s}. \tag{12}$$

R_m , R_a , R_c , and R_s above are the aortic, atrial, characteristic, and systemic resistances, respectively. C_a , C_r , and C_s are the aortic, left atrial, and systemic compliances. U_{mi} and U_{ao} are used for mitral and aortic disorders, respectively. They are described in Section 2.4 further below.

2.3. Electrico-Chemical Model

The electrophysiology is represented by the parameters p and q representing slow and fast electrical activity. Equations (13) and (14) below govern these variables, and Equation (15) describes the evolution of the chemical activity u which is proportional to the fast electrical activity variable q .

$$\frac{dp}{dt} = 0.1(q - p + \mu_1 \tau_c), \tag{13}$$

$$\frac{dq}{dt} = 10q(1 - q^2) - 10(2\pi)^2 p + \mu_2 V_+ + 10 \cos(2\pi t), \tag{14}$$

$$u = \alpha_u q. \tag{15}$$

The constant parameters μ_1 and μ_2 model the MEF. Kim and Capoccia [32] describe μ_1 as mimicking systolic mechanical stretch, whereas μ_2 mimics diastolic stretch. Increasing either parameter increases the coupling between electrical and mechanical parts of the model, thereby increasing the stretch of the MEF. For further detail regarding these parameters and their effects, refer to [28,32,33]. The last term, $10 \cos(2\pi t)$ in Equation (14), simulates the heart rate (1 Hz) in the control case.

2.4. Valve Disorders

In the circulation equations above, two constant parameters U_{mi} and U_{ao} are used. U_{mi} describes disorders of the mitral valve and U_{ao} disorders of the aortic valve. In a ‘healthy’ heart without a disorder of either valve, both parameters are 1 when the preceding term is positive and 0 otherwise. For example, U_{mi} is 1 when $(P_r - P_v)$ is positive and 0 otherwise. Likewise U_{ao} is 1 when $(P_v - m)$ is positive and 0 otherwise. Different valves may be used to represent a valve pathology. For a stenosis, instead of U_{mi} and U_{ao} being 1 or 0, the 1 can be reduced, but 0 stays the same. To represent valve regurgitation, instead of U_{mi} and U_{ao} being 1 or 0, the 0 value can be increased depending on severity, but the value 1 must remain. Table 4 provides the values used for modelling different severities of each valve disorder. For a stenosis, the values represent the proportion of flow unobstructed. Therefore, the mild case represents a 30% flow restriction, the moderate case represents 50% restriction and the severe case represents 90% restriction. This covers a similar range of flow restriction to [16]. The values used for valve regurgitation are also identical to [16]

who use a similar method to model valve disorders, and use the clinical definitions for regurgitation severity.

Table 4. Mitral and aortic valve pathology values. The different values provided in the table are applied to U_{mi} and U_{ao} to simulate different severities of valve pathologies. Refer to Section 2.4 for an explanation of how this is done. For stenosis, 0.7, 0.5, and 0.1 represent 30, 50, and 90% flow restriction. For regurgitation, the values are identical to [16] who use the clinical definition of regurgitation severity.

Disorder	Mild	Moderate	Severe
Stenosis	0.7	0.5	0.1
Regurgitation	0.004	0.024	0.05

The equivalent electrical diagram for the complete model just described is shown in Figure S1 in the Supplementary Materials section. The physiological meaning of the model variables is given in Table 1. The parameter values for the micro-scale mechanical and electrical models in Table 2 are those used by [28,33], and those for the macro-scale circulation model in Table 3 are provided by [39]. The system of Equations (1)–(15) are solved in Matlab R2021a (Mathworks) using a custom written fourth-order Runge–Kutta scheme and the accuracy of the numerical solution is checked by systematically reducing the time-step until differences between results become negligible.

3. Results

3.1. Mitral Valve Pathology

We first examine the effects of mitral valve pathologies without a dysfunction of the MEF. Figure 1a shows left ventricle pressure–volume loops (P-V) for the different severities of mitral valve stenosis recorded in Table 4. The loops can be seen to progressively shift downward and to the left as the severity worsens. The reduction in orifice area causes the end-systolic and diastolic pressures and volumes to fall, as does P_V overall. Figure 1b,c show that as the stenosis worsens, the cardiac output and stroke volume reduce. The end-diastolic and systolic volumes (EDV and ESV) shift to the left; the EDV by 7 mL and the ESV by 1.5 mL. This is similar in degree to [16] who see a 5 mL shift in the EDV and 3 mL for the ESV between the mild and severe cases. The downward shift of the systolic and diastolic pressures is also similar. Figure 2a shows there is slight reduction in systemic pressure P_s , and Figure 2b shows there is an increase in the atrial pressure P_r .

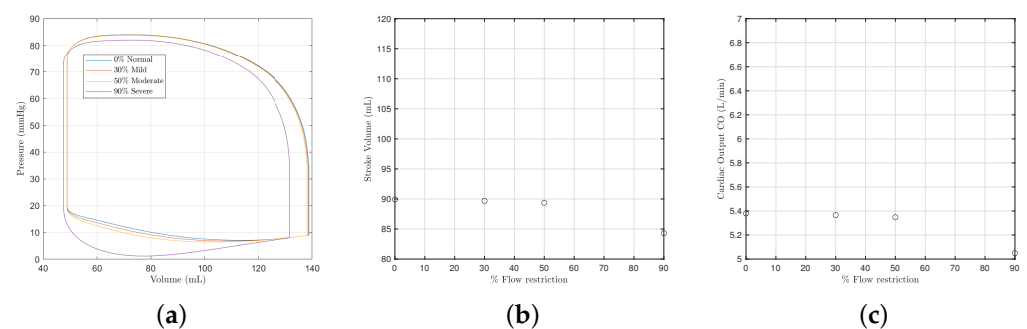


Figure 1. The left ventricle pressure–volume loop, the stroke volume, and the cardiac output with different severities of mitral valve stenosis. The model parameter values used to model each severity are provided in Table 4. (a) Pressure–volume loops. (b) The stroke volume SV. (c) The cardiac output CO.

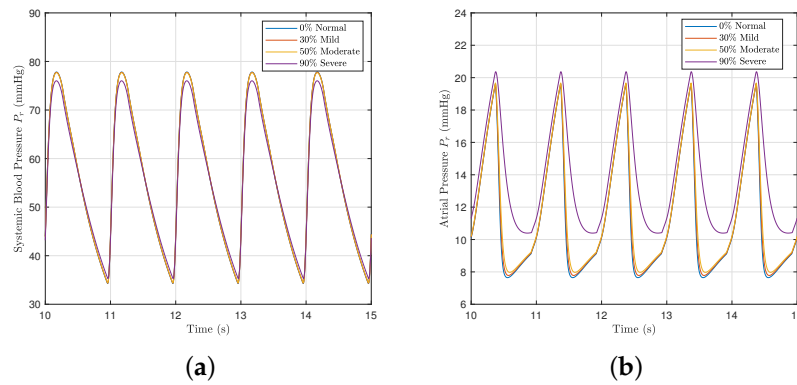


Figure 2. The systemic and atrial pressures with different severities of mitral valve stenosis. (a) Systemic blood pressure P_s . (b) Atrial pressure P_r .

Figure 3a shows the effects of mitral valve regurgitation on the left ventricle P-V loops for different severities of regurgitation. As the disease worsens, the systolic pressure falls as new flow is pumped back into the atrium, and the loops widen with an elimination of the isovolumic phases. Consequently, the stroke volume and cardiac output displayed in Figure 3b,c rise as the left-ventricle is enlarged [40]. The x axis of the figures give the severity of regurgitation, where 1 denotes normal or control, 2 denotes mild, 3 denotes moderate, and 4 denotes severe. The model parameter values used to model each severity are provided in Table 4. The degree of changes displayed in Figure 3a agree well with [16,41].

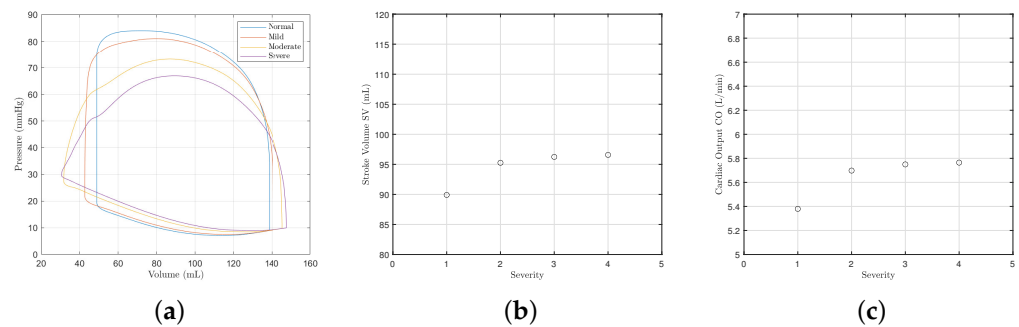


Figure 3. Left ventricle pressure–volume loop, the stroke volume and the cardiac output with different severities of mitral valve regurgitation. The x axis of the SV and CO figures give the severity of regurgitation, where 1 denotes normal or control, 2 denotes mild, 3 denotes moderate, and 4 denotes severe. The model parameter values used to model each severity are provided in Table 4. (a) Pressure–volume loops. (b) The stroke volume. (c) The cardiac output.

Figure 4 shows how different severities of mitral valve regurgitation affect the model variables. As the severity of mitral valve regurgitation worsens, the systemic pressure falls further as more blood flows back through the mitral valve and less downstream. The atrial pressure P_r consequently increases too due to the rise in blood back-flow. The aortic pressure m reduces for the same reason that the systemic pressure falls too.

3.2. Aortic Valve Pathology

Aortic valve pathologies make up the majority of valve disorders leading to mortalities. The effect of aortic valve stenoses corresponding to Table 4 on the left ventricular P-V loops is shown in Figure 5a. As the disease progresses, there is a slight increase in systolic pressure and end-systolic volume though some clinical reports suggest the change should be greater [42]. Figure 5b,c show, respectively, the corresponding reduction in stroke volume and cardiac output. Despite the severity of the stenosis, the effects for the aortic

valve appear to be very mild compared to mitral valve stenosis. Not shown is that there is slight reduction in systemic blood pressure P_s and an increase in atrial pressure P_r .

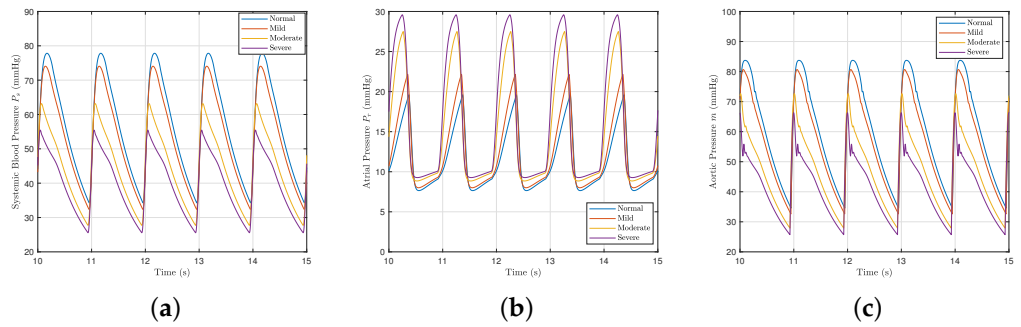


Figure 4. The systemic, atrial, and aortic pressures with different severities of mitral valve regurgitation. (a) Systemic blood pressure P_s . (b) Atrial pressure P_r . (c) Aortic pressure m .

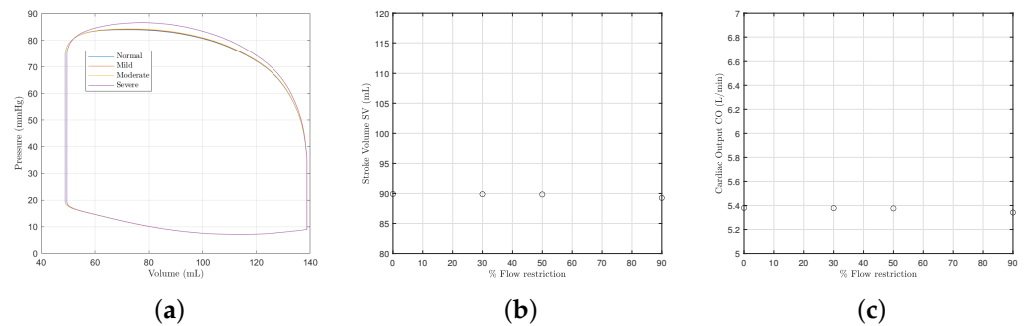


Figure 5. Left ventricle pressure–volume loop, the stroke volume and the cardiac output with different severities of aortic valve stenosis. (a) Pressure–volume loops. (b) The stroke volume. (c) The cardiac output.

Figure 6a shows the effect of aortic valve regurgitation on the ventricle P-V loops. The stroke volume increases (Figure 6b) as the loops widen, as does cardiac output (Figure 6c). The widening of the loops is largely as a result of the end-diastolic volume (preload). The systolic pressure decreases, the diastolic pressure rises, and the isovolumetric phases become curved. As shown in Figure 7, the atrial pressure rises, whilst the systemic and aortic blood pressures fall. The change for aortic regurgitation found here more closely matches published literature [42,43].

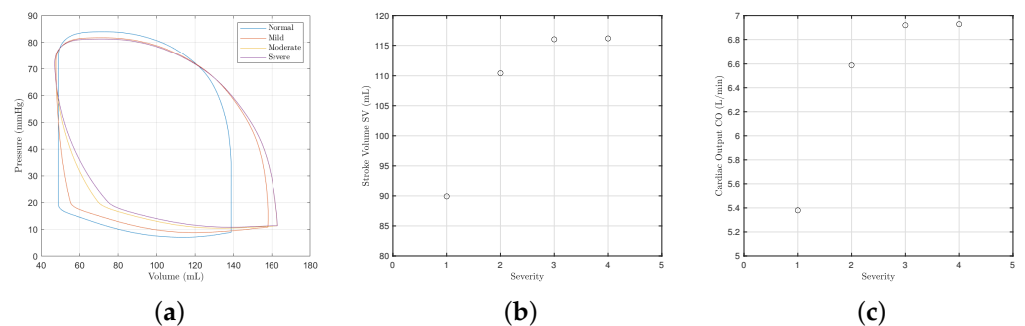


Figure 6. Left ventricle pressure–volume loop, the stroke volume and the cardiac output with different severities of aortic valve regurgitation. The x axis of the SV and CO figures give the severity of regurgitation, where 1 denotes normal or control, 2 denotes mild, 3 denotes moderate, and 4 denotes severe. The parameter values used to model each severity are provided in Table 4. (a) Pressure–volume loops. (b) The stroke volume. (c) Cardial output.

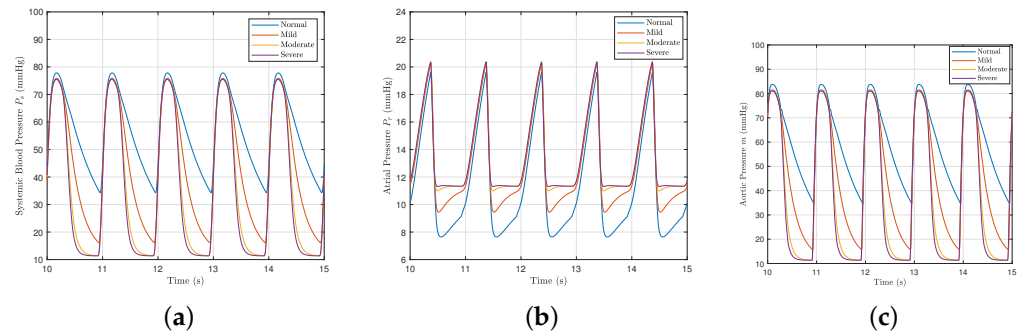


Figure 7. Systemic, atrial, and aortic pressures with aortic valve regurgitation. (a) Systemic blood pressure P_s . (b) Atrial pressure P_r . (c) Aortic pressure m .

3.3. Valve Motion

Before exploring the impact of valve disorders on the MEF, a brief examination of valve motion is made. To model valve motion, U_{mi} and U_{ao} are modified to produce a simple valve motion. For mitral valve opening then closing, the following is applied for the mitral valve

$$U_{mi} = \cos \theta, \quad P_r \geq P_v \tag{16}$$

$$U_{mi} = 1 - \cos \theta, \quad P_r < P_v \tag{17}$$

Likewise for the aortic valve,

$$U_{ao} = \cos \theta, \quad P_v \geq m \tag{18}$$

$$U_{ao} = 1 - \cos \theta, \quad P_v < m \tag{19}$$

where θ is a linear vector running from 90° to 0° . The angle θ may be thought of as being aligned with the direction of flow. The model above is far simpler than comparable low order models such as that used by [44] who also consider local flow effects around the valve, but it still allows for an exploration of valve opening and closing times. The time may be controlled by adjusting the speed with which θ completes its motion. It could also be used for an alternative way to model valve disorders too by adjusting the final value of θ . Figure 8 shows the effects of mitral valve opening and closing times on the pressure–volume loop. It can be seen that the closing time of the mitral valve has a much greater effect on the P-V loop than the opening time and the longer the closing time, the greater the effect. The two plots in Figure 8 show the change in the variable U_{mi} . We refer the reader to Section 2.4 for an explanation of U_{mi} . The opening time of the valve does not appear to affect the closing time, but the closing time does affect the opening time of the next heart beat.

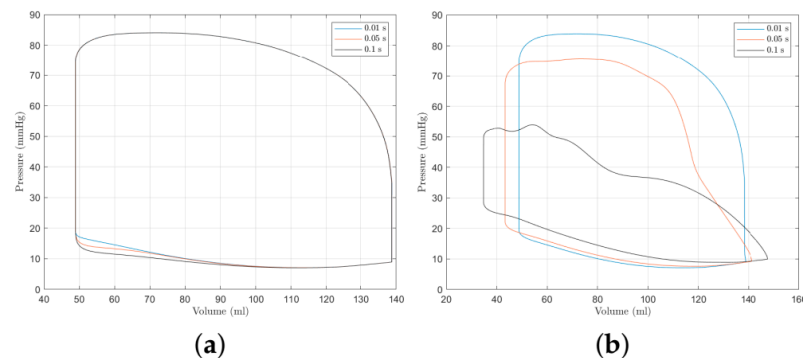


Figure 8. Cont.

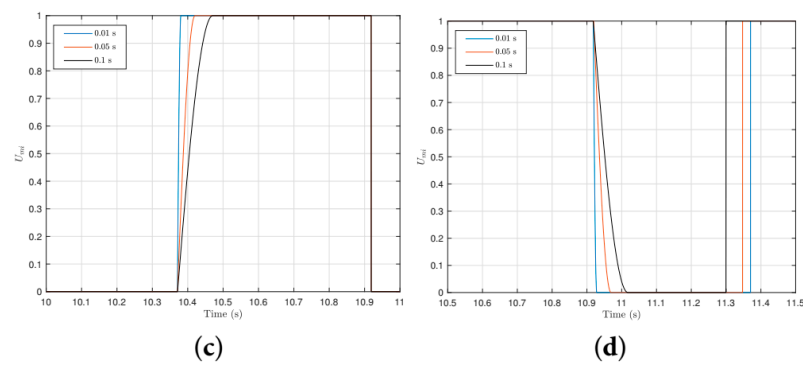


Figure 8. The effect of mitral valve opening and closing time. (a,b) show, respectively, the effect of opening and closing time on the P-V loop, respectively, and (c,d) show traces of U_{mi} for different opening and closing times (refer to Section 2.4 for an explanation of U_{mi}). (a) The effect of mitral valve opening time on the P-V loop. (b) The effect of mitral valve closing time on the P-V loop. (c) Time traces of U_{mi} for different opening times. (d) Time traces of U_{mi} for different closing times.

Figure 9 shows the effect of the aortic valve opening and closing times on the P-V loop with corresponding traces of the variable U_{ao} . From Figure 9, a similar conclusion can be made about the aortic valve as the mitral valve in that the valve closing time has a much greater impact on model behaviour than the opening time. To produce a similar model behaviour to the control-case (representing a typical ‘healthy’ person), the closing time of the left-ventricle valves must be short. This is similar to the observation by [44] who find that valve motion is brief and abrupt. Using their valve model, Korakianitis et al. [44] find that the entire valve opening and closing process takes 0.1 s. Using the cardiac model here, the closing time should make up a far smaller proportion of the 0.1 s. In the remainder of this study, valve motion is modelled as being instantaneous so that the focus remains on the MEF.

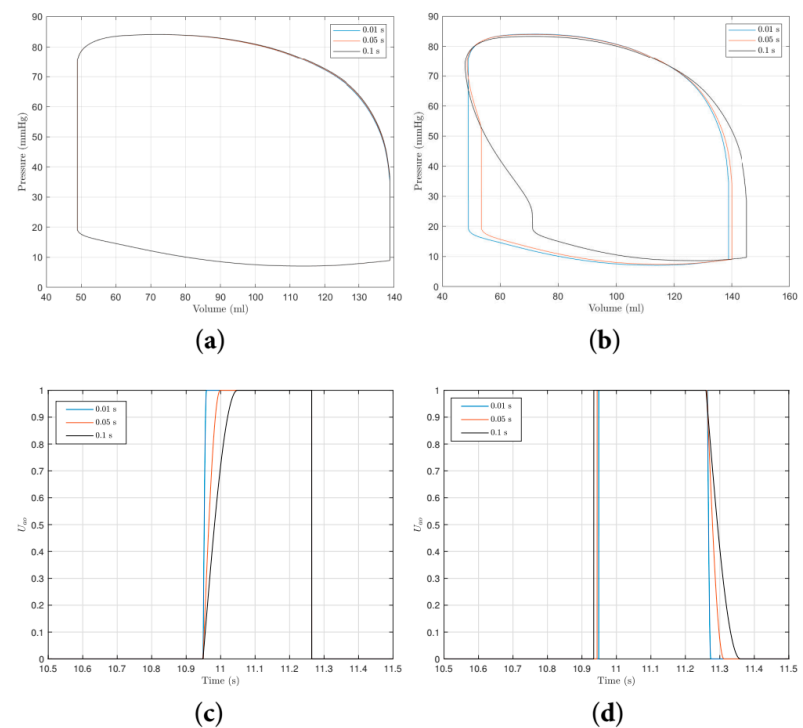


Figure 9. The effect of aortic valve opening and closing time. (a,b) show, respectively, the effect of aortic valve opening and closing time on the P-V loop, and (c,d) show traces of U_{ao} for different opening and closing times (refer to Section 2.4 for an explanation of U_{ao}). (a) The effect of aortic valve opening time on the P-V loop. (b) The effect of aortic valve closing time on the P-V loop. (c) Time traces of U_{ao} for different opening times. (d) Time traces of U_{ao} for different closing times.

3.4. MEF

The response of MEF dysfunction to valve stenoses and regurgitation are now explored using the current model (without valve motion) by increasing the MEF parameters μ_1 and μ_2 with the addition of valve disorders. Kim and Capoccia [32] conduct a comparable study using a similar model without valve pathology. Figure S2 in the Supplementary Materials section shows the effects of increasing μ_1 for the control case in the model here without valve disorders. When $\mu_1 = 0.0128$ period doubling occurs, as shown in the top row of Figure S2. In the second row, when $\mu_1 = 0.0145$, 5 P-V loops can be seen which falls to 3 in the third row ($\mu_1 = 0.02$) and finally a single loop when $\mu_1 = 0.0268$. As noted above, the MEF parameter μ_1 couples the slow activity variable p to ventricular stress τ_c . As the stress is greatest during systole, μ_1 mimics the effect of systolic mechanical stress (stretch) on the excitation wave. As μ_1 is increased, the sensitivity to systolic stretch increases, causing the end-diastolic and systolic volumes to rise. The heart rate (hr) falls, showing that missed beats occur with increasing frequency as μ_1 rises. The mean CO consequently reduces due to the reduction in hr. The slow electrical activity p increases faster to greater values, but falls more gradually which prolongs the repolarisation process causing a longer action potential (AP duration or APD); an effect also seen by Kim and Capoccia [32] and noted by others [12,23,45].

The MEF parameter μ_2 couples the faster depolarisation electrical activity variable (represented here by q) to a rise in ventricular volume V , thereby mimicking the effect of diastolic mechanical stretch. A rise in μ_2 increases the sensitivity to diastolic stretch. Figure S3 in the Supplementary Materials section shows the effects of increasing μ_2 as $\mu_2 = [0.1530, 0.1584, 0.1718, 0.36, 1.8]$ on the control case ($\mu_1 = 0.0024$). Stretch during diastole causes SACs to open, allowing currents to flow into the cell which depolarises the action potential causing contraction [23,34]. Hence, the heart rate increases substantially, reaching 193 bpm when $\mu_2 = 1.8$. The stroke volume declines as the EDV reduces while the ESV rises. Despite the reduction in stroke, the CO rises; presumably due to the rapid rise in heart rate. Unlike systolic stretch, no periodic behaviour is seen. Instead, μ_2 gives rise to complex P-V loops. The maximum value of the fast activity q shown in the last figure column can be seen to increase, whilst that of p reduces. This suggests that the AP depolarisation is stronger, and the repolarisation process weaker, hence the APD reduces. Unlike μ_1 , increasing μ_2 does not produce similar periodic behaviour as is evident from the figures.

3.4.1. Effect of μ_1 ($\mu_2 = 0$) with Mitral Valve Pathology

The parameter μ_1 is progressively increased ($\mu_2 = 0$) for the cases with a severe mitral valve stenosis or regurgitation, respectively, (refer to Table 4 for severity). In order to determine the effects of each pathology in the presence of MEF dysfunction, the average heart rate (hr), SV, and CO are compared with the control case. The value of μ_1 at which periodic behaviour occurs is also compared. With a severe mitral valve disorder, instead of 2, 5, 3, and 1 P-V loops only 2, 4, 3, and 1 occur. Table 5 shows the results with the headings 2, 4 or 5, 3, and 1 representing two, four or five, three, and one P-V loops.

It can be seen that the sensitivity to systolic stretch is increased slightly with mitral valve stenosis, as the value of μ_1 at which period doubling occurs is lower for stenosis. This is consistent with experimental studies of the mitral valve that the rise in arrhythmia occurrences with mitral valve stenosis is due to higher atrial pressures, and an increase in intraventricular volume [46]. With a mitral valve regurgitation, period doubling occurs at a larger value of μ_1 compared to the control case. Sensitivity to systolic stretch can therefore be concluded to reduce when mitral valve regurgitation is present. However, mitral valve pathology does not alter the effect of μ_1 . As μ_1 increases, the SV, tends to increase but the hr and CO both tend to decline as they did for the control case. The reduction in CO in particular shows how the MEF can lead to cardiac problems and even death, as the pumping power of the heart diminishes.

Table 5. Effect of μ_1 with a severe mitral valve stenosis or regurgitation. Refer to Table 4 for severity. μ_1 increases from left to right. The headings 2, 4 or 5, 3, and 1 denote the number of P-V loops appearing in the P-V plot as μ_1 is increased. The results given in the μ_1 rows give the values of μ_1 at which the 2, 4 or 5, 3, and 1 P-V loops are observed. SV, CO, and hr rows likewise provide the stroke-volume, cardiac output, and heart rate measured at that value of μ_1 .

Control	2	5	3	1
μ_1	0.0128	0.0145	0.02	0.0268
SV	70.8	70.2	74.0	90.4
CO	4.2	3.7	3.5	2.7
hr	1.0	0.96	0.82	0.50
Stenosis	2	4	3	1
μ_1	0.0118	0.0126	0.0190	0.0235
SV	61.1	56.9	71.5	91.1
CO	3.7	3.1	3.3	2.7
hr	1.08	1.12	0.83	0.50
Regurgitation	2	4	3	1
μ_1	0.0196	0.0225	0.385	0.055
SV	86.7	75.1	87.5	100.6
CO	5.3	4.3	4.1	3.0
hr	1.03	1.09	0.80	0.50

3.4.2. Effect of μ_1 ($\mu_2 = 0$) with Aortic Valve Pathology

μ_1 is now progressively increased with aortic valve pathologies in a similar fashion to the mitral valve. The results are tabulated in Table 6 along with the control case for comparison. Overall, the effects of μ_1 are quite similar to the changes seen for the mitral valve and control cases. The end-diastolic and systolic volumes rise, the hr tends to fall as does the CO. Again the reductions in hr and CO show the damaging effects of the MEF. As μ_1 at which period doubling first appears is slightly larger with an aortic valve stenosis or regurgitation than that without, a reduction in sensitivity to systolic stretch can be said to result from aortic valve disorders.

Table 6. Effect of μ_1 with a severe aortic valve stenosis or regurgitation. Refer to Table 4 for severity. μ_1 increases from left to right. The headings 2, 4 or 5, 3, and 1 denote the number of P-V loops appearing in the P-V plot as μ_1 is increased. The results given in the μ_1 rows give the values of μ_1 at which the 2, 4 or 5, 3, and 1 P-V loops are observed. SV, CO, and hr rows likewise provide the stroke-volume, cardiac output, and heart rate measured at that value of μ_1 .

Control	2	5	3	1
μ_1	0.0128	0.0145	0.02	0.0268
SV	70.8	70.2	74.0	90.4
CO	4.2	3.7	3.5	2.7
hr	1.0	0.96	0.82	0.50
Stenosis	2	4	3	1
μ_1	0.13	0.0182	0.0220	0.0280
SV	69.6	67.1	70.7	87.8
CO	4.1	3.3	3.3	2.6
hr	0.99	0.92	0.82	0.50
Regurgitation	2	4	3	1
μ_1	0.0164	0.0270	0.0315	0.0550
SV	87.4	76.3	77.7	81.1
CO	5.18	3.86	3.59	2.44
hr	1.0	0.90	0.81	0.50

3.4.3. Effect of μ_2 ($\mu_1 = 0.0024$) with Mitral Valve Pathology

μ_1 is returned to its control value $\mu_1 = 0.0024$, and μ_2 is gradually increased with a severe mitral valve disorder (see Table 4 for severity). As noted in the control case above, μ_2 does not produce periodic behaviour similar to μ_1 . The same values of μ_2 are therefore compared between all cases. Specifically, μ_2 is chosen to be $\mu_2 = [0.1530, 0.1584, 0.1718, 0.36, 1.8]$ for all the cases with or without a valve disorder. The results are tabulated in Table 7 with μ_2 increasing from left to right columns. The effects of μ_2 on the ventricle are unchanged regardless of mitral valve disease. Ectopic beats appear and the heart rate increases as before. We note that the P-V loop in the control case without a valve pathology begins to bifurcate and show different loop shapes when $\mu_2 = 0.1516 \sim 0.1517$. That is for any $\mu_2 < 0.1516$, the P-V loop appears normal and representative of a ‘healthy’ person. With a severe mitral valve stenosis, the P-V loops begin to bifurcate when $\mu_2 \approx 0.1528$, hence mitral valve stenosis can be concluded to reduce the sensitivity to arrhythmia stimulating diastolic stretch. This is also evident in the hr, which does not increase to the same extent as the control case.

With a severe mitral valve regurgitation, the first appearance of bifurcation occurs when $\mu_2 = 0.1516 \sim 0.1517$, which is identical to the case without valve pathology. Despite this result, the hr with regurgitation is increased immediately when diastolic stretch ($\mu_2 \neq 0$) is introduced. Regurgitation also increases the hr at a greater rate compared to both the control case and mitral valve stenosis. The mechanism behind this result is evident in Equation (14). That is, mitral valve regurgitation produces a much wider diastolic stroke and a larger stroke volume. This increases the stretch (increase in volume) during this period, leading to a rise in ectopic beats and hr. Ventricular arrhythmia will therefore be more likely with valve regurgitation, with the greater the severity of regurgitation, the more severe the arrhythmia. This result should be expected when aortic valve regurgitation is present too as the stroke volume is larger again. These results are consistent with clinical studies which show that the severity of regurgitation is an indicator for the degree of complications experienced during cardiac arrhythmia [47–49].

Table 7. Effect of μ_2 with a severe mitral valve stenosis or regurgitation.

μ_2	0.153	0.1584	0.1718	0.36	1.8
Control					
SV	78.8	72.3	66.8	45.2	32.3
CO	5.10	5.24	5.45	6.05	6.2
hr	1.04	1.26	1.41	2.25	3.22
Stenosis					
SV	78.3	71.4	64.8	46.6	37.5
CO	4.83	4.85	4.89	5.03	4.8
hr	1.04	1.17	1.32	1.84	2.20
Regurgitation					
SV	75.7	73.1	71.1	57.0	40.8
CO	6.11	6.45	7.40	10.32	11.52
hr	1.49	1.60	1.80	3.02	4.73

3.4.4. Effect of μ_2 ($\mu_1 = 0.0024$) with Aortic Valve Pathology

With the parameter μ_1 returned to its control value ($\mu_1 = 0.0024$), the value of μ_2 is increased with the addition of aortic valve pathology in a similar way to the control case (as $\mu_2 = [0.1530, 0.1584, 0.1718, 0.36, 1.80]$). Table 8 documents the results. A similar behaviour pattern to the case of the mitral valve pathology appears as μ_2 increases. The value at which bifurcation first appears is $\mu_2 \approx 0.152$ which is similar to the control case hence, sensitivity to diastolic stretch is unaffected by aortic stenosis. With severe aortic regurgitation, the value at which bifurcation first appears is $\mu_2 \approx 0.1515$. As expected, when aortic valve

regurgitation is present and $\mu_2 \neq 0$, ectopic beats become far more frequent, leading to a faster hr. Furthermore, the hr increases at a greater rate as μ_2 rises, in agreement with findings above.

Table 8. Effect of μ_2 with a severe aortic valve stenosis or regurgitation.

μ_2	0.153	0.1584	0.1718	0.36	1.8
Control					
SV	78.8	72.3	66.8	45.2	32.3
CO	5.10	5.24	5.45	6.05	6.2
hr	1.10	1.26	1.41	2.25	3.22
Stenosis					
SV	81.6	73.0	65.9	45.2	32.0
CO	4.93	5.15	5.30	5.99	6.14
hr	1.01	1.24	1.43	2.22	3.22
Regurgitation					
SV	91.8	86.5	85.5	74.4	45.6
CO	8.67	8.55	9.42	12.89	13.94
hr	1.61	1.68	1.86	2.88	5.10

4. Discussion

Our aim was to develop a new model by extending a synergistic reduced-order mathematical model of the cardiovascular system [28] to include the effects of pathologies in the valves of the left-ventricle; the mitral valve and the aortic valve. A further aim was to see what effect if any, valve pathologies have on (disorders of) the mechano-electric physiology of the heart. In order to meet the latter aim, the popular time-varying elastance method of generating the pressure–volume relationship could not be applied. The TVE method uses a periodic function to generate the pressure–volume relationship rather than calculating it consistently, hence it cannot be used to simulate the feedback mechanisms which maintain cardiac stability, most notably the MEF. It has frequently been questioned both due to its empirical foundations and validity for cardiac modelling [17,31]. The synergistic model [28] develops the organ scale dynamics of pressure and volume from the micro-scale activity of the myocytes. Since it encompasses the mechanical, electrical and chemical domains it can be used to simulate the MEF. The model is modified to include stenoses and regurgitation in the heart’s mitral and aortic valves, modelling different severities of different valve disorders.

Mitral valve stenosis without a dysfunction of the MEF is found to cause a reduction in ventricular and systemic pressures and reduction in the cardiac output and stroke volume. The atrial pressure increases slightly. The EDV and ESV both reduce, shifting the P-V loop to the right. The extent of this reduction and shift is of similar order to [16] for a comparable range of severity. The results with mitral regurgitation show that the P-V loop widens, enlarging the ventricle, increasing the stroke volume, cardiac output, and myocardial load in agreement with medical reports [40]. The degree of the changes in the ventricle agrees well with [16,41]. The atrial pressure rises whilst the systemic blood pressure falls. For aortic valve stenosis, the ventricular pressure rises but this rise is very minor, even with 90% flow restriction. The stroke volume and cardiac output reduce but again, this reduction is very minor. Aortic valve regurgitation has a greater effect and agrees with published literature [43]. Like the mitral valve, the stroke volume and cardiac output rise. This is due to an increase in the end-diastolic volume and slight decrease in end-systolic volume. The systemic blood pressure falls significantly during diastole, but the atrial pressure rises.

Dysfunction of the MEF is modelled by increasing the coupling between the mechanical part of the model and the electrical. Two parameters are used for this coupling; μ_1 and μ_2 . The former mimics the effect of mechanical ventricular stretch during systole and the latter mimics the effect stretch during diastole. By increasing these parameters,

dysfunctions of the MEF can be simulated and the effects on the cardiovascular system investigated. See [32,33] for their effects without valve disorders. A dysfunction of the MEF is investigated here with the addition of severe disorders in the mitral and aortic valves. Disorders in the mitral and aortic valves do not qualitatively change the overall effects of the MEF parameters. The parameter μ_1 mimicking systolic stretch causes a reduction in the electrical activity, leading to missed heartbeats and a reduction in the pumping power of the heart, and is unaffected by disorders in the aortic and mitral valves. The parameter μ_2 mimicking diastolic stretch causes an increase in the electrical activity leading to ectopic beats and complex pressure–volume behaviour. This too is unaffected by disorders in the valves of the left ventricle.

Valve disorders do however have quantitative effects. Specifically, they change the sensitivity of the heart to arrhythmia-stimulating stretch. Sensitivity to systolic stretch is compared between cases by looking at the value of μ_1 at which period doubling occurs. The lower the value of μ_1 when periodic behaviour appears, the greater the sensitivity to systolic stretch. Mitral valve stenosis slightly increases the sensitivity to systolic stretch while regurgitation reduces it to a greater extent. Neither stenosis nor regurgitation affect the number and frequency of ectopic beats and the heart rate remains the same as the control case. Aortic valve stenosis does not change the sensitivity to systolic stretch, and regurgitation decreases it, as the value of μ_1 is larger than the control case. Similar to the mitral valve, pathologies in the aortic valve do not change the frequency of missed beats.

Sensitivity to diastolic stretch is compared between cases by finding the approximate value of μ_2 at which the results begin to bifurcate. Again, a lower value of μ_2 is indicative of increased sensitivity. Cases are also compared for similar values of μ_2 , such that the same level of diastolic stretch is applied. Mitral stenosis slightly reduces sensitivity to arrhythmia stimulating diastolic stretch while aortic stenosis has no effect. Stenosis in either valve does not change the heart rate rise resulting from the MEF. Mitral and aortic valve regurgitation do not affect the sensitivity to diastolic stretch. Furthermore, we find that valve regurgitation increases the heart rate and frequency of ectopic beats resulting from diastolic stretch. This applies whenever $\mu_2 \neq 0$ and valve regurgitation is introduced. The mechanism behind this result is found to be the increase in myocardial load and diastolic stroke resulting from regurgitation. The diastolic stretch is therefore longer and larger. Arrhythmia (ectopic beats, irregular heart rate) resulting from MEF dysfunction will therefore be more severe. This result agrees very well with clinical results showing that the severity of regurgitation is an indicator for the complications experienced during arrhythmia [47–49].

Limitations of the model: The model inherits the same limitations as the model by Kim and Capoccia [28], namely that the 0-dimensional lumped-parameter nature does not allow for wave dynamics in the electrical and cellular behaviour to be modelled. This could limit the investigation of the MEF in which wave dynamics can have a significant effect. Another weakness is the simple electro-chemical model. This model cannot be used to identify the specific ion channels involved in the pattern of cellular excitation.

5. Conclusions

This study describes the successful modification and use of the cardiovascular mathematical model developed by Kim and Capoccia [28,32] to study the effects of the pathologies in the mitral and aortic valves. The effects of valve pathologies on the MEF is additionally studied. Mitral valve stenosis increases the sensitivity to arrhythmia-stimulating systolic stretch, but reduces the sensitivity to diastolic stretch. Aortic valve stenosis does not change the sensitivity to arrhythmia-stimulating stretch, and regurgitation reduces it. No significant effect on the sensitivity to diastolic stretch is found for the aorta. A key result is found when valve regurgitation is accompanied by diastolic stretch. Whilst diastolic stretch increases the number of ectopic beats in the presence of MEF disorder, the ectopic beats become far more frequent when accompanied by valve regurgitation. Arrhythmia resulting from a disorder in the MEF will therefore be more severe when valve regurgitation

is present, and the more severe the regurgitation the more serious the arrhythmia. This finding agrees well with published clinical literature. A possible mechanism responsible for the rise in the number of ectopic beats is provided.

Finally, we demonstrated how to incorporate valve opening and closing times within our model, indicating some potentially interesting results. It remains a future work to perform detailed analysis on valve motion. It would be also be interesting to extend our study to a continuous model such that the effects of wave dynamics can be studied, particularly in the context of MEF. Extending the electrical model to include a more detailed description of the cellular ion channels is also of interest as the particular channels involved in generating a significant MEF effect can be better studied.

Supplementary Materials: The following supporting information can be downloaded at: <https://www.mdpi.com/article/10.3390/bioengineering9090454/s1>, Figure S1: The equivalent electrical diagram of the complete cardiovascular system described. For abbreviation definitions refer to Table 3. The left atrium feeds blood at a pressure P_r through the mitral valve (the diode) into the left ventricle (L_v). As the blood passes through the valve it encounters a resistance R_m . With the mitral valve closed the aortic valve (second diode) opens allowing blood at pressure P_v to flow into aorta encountering a valve resistance R_a . The aorta has a compliance C_a . The aortic blood at pressure m flows (F_a) towards the remainder of the body encountering a characteristic resistance R_c . The blood has an inertia L_s due to its mass and encounters the resistance R_s and compliance C_s of the body's systemic arteries and tissues. The blood at pressure P_s after feeding the organs with fresh oxygen and nutrients is re-oxygenated and flows back to left atrium (with compliance C_r) ready for another cycle. Figure S2: The effect of increasing μ_1 for the control case: $\mu_1 = [0.0128, 0.0145, 0.020, 0.0268]$. Figure S3: The effect of increasing μ_2 for the control case: $\mu_2 = [0.153, 0.1584, 0.1718, 0.36, 1.8]$.

Author Contributions: Conceptualization, N.P. and E.-j.K.; methodology, N.P. and E.-j.K.; formal analysis, N.P.; writing, N.P. and E.-j.K.; supervision, E.-j.K. All authors have read and agreed to the published version of the manuscript.

Funding: This research received no external funding.

Conflicts of Interest: The authors declare no conflict of interest.

References

1. Nkomo, V.T.; Gardin, J.M.; Skelton, T.N.; Gottdiener, J.S.; Scott, C.G.; Enriquez-Sarano, M. Burden of valvular heart diseases: A population-based study. *Lancet* **2006**, *368*, 1005–1011. [CrossRef]
2. Centers for Disease Control and Prevention. National Center for Health Statistics. CDC WONDER Online Database. 2018. Available online: <http://wonder.cdc.gov/ucd-icd10.html> (accessed on 23 May 2022).
3. Basso, C.; Perazzolo Marra, M.; Rizzo, S.; De Lazzari, M.; Giorgi, B.; Cipriani, A.; Frigo, A.C.; Rigato, I.; Migliore, F.; Pilichou, K.; et al. Arrhythmic mitral valve prolapse and sudden cardiac death. *Circulation* **2015**, *132*, 556–566. [CrossRef]
4. Perazzolo Marra, M.; Basso, C.; De Lazzari, M.; Rizzo, S.; Cipriani, A.; Giorgi, B.; Lacognata, C.; Rigato, I.; Migliore, F.; Pilichou, K.; et al. Morphofunctional abnormalities of mitral annulus and arrhythmic mitral valve prolapse. *Circ. Cardiovasc. Imaging* **2016**, *9*, e005030. [CrossRef] [PubMed]
5. Orini, M.; Nanda, A.; Yates, M.; Salvo, C.D.; Roberts, N.; Lambiase, P.D.; Taggart, P. Mechano-electrical feedback in the clinical setting: Current perspectives. *Prog. Biophys. Molec. Biol.* **2017**, *130*, 365–375. [CrossRef] [PubMed]
6. Noseworthy, P.A.; Asirvatham, S.J. The knot that binds mitral valve prolapse and sudden cardiac death. *Circulation* **2015**, *132*, 551–552. [CrossRef] [PubMed]
7. Levy, S. Factors Predisposing to the Development of Atrial Fibrillation. *Pacing Clin. Electrophysiol.* **1997**, *20*, 2670–2674. [CrossRef]
8. Quarteroni, A.; Lassila, T.; Rossi, S.; Ruiz-Baier, R. Integrated Heart—Coupling multiscale and multiphysics models for the simulation of the cardiac function. *Comput. Methods Appl. Mech. Eng.* **2017**, *314*, 345–407. [CrossRef]
9. Kohl, P.; Hunter, P.; Noble, D. Stretch-induced changes in heart rate and rhythm: Clinical observations, experiments and mathematical models. *Biophys. Mol. Biol.* **1999**, *71*, 91–138. [CrossRef]
10. Link, M.S.; Wang, P.J.; Pandian, N.G.; Bharati, S.; Udelson, J.E.; Lee, M.Y.; Vecchiotti, M.A.; VanderBrink, B.A.; Mirra, G.; Maron, B.J.; et al. An experimental model of sudden death due to low-energy chest-wall impact (commotio cordis). *N. Engl. J. Med.* **1998**, *18*, 1805–1811. [CrossRef]
11. Link, M.S.; Wang, P.J.; VanderBrink, B.A.; Avelar, E.; Pandian, N.G.; Maron, B.J.; Estes, N.M., III. Selective activation of the K^+ ATP channel is a mechanism by which sudden death is produced by low-energy chest-wall impact (commotio cordis). *Circulation* **1999**, *100*, 413–418. [CrossRef]

12. Knudsen, Z.; Holden, A.; Brindley, J. Qualitative modeling of mechano-electrical feedback in a ventricular cell. *Bull. Math. Biol.* **1997**, *6*, 115–181.
13. Hazim, A.; Belhamadia, Y.; Dubljevic, S. Effects of mechano-electrical feedback on the onset of alternans: A computational study. *Chaos* **2019**, *29*, 063126. [[CrossRef](#)] [[PubMed](#)]
14. Maron, B.J.; Link, M.S.; Wang, P.J.; Estes, N.A., 3rd. Clinical profile of commotio cordis: An under appreciated cause of sudden death in the young during sports and other activities. *J. Cardiovasc. Electrophysiol.* **1999**, *10*, 114–120. [[CrossRef](#)] [[PubMed](#)]
15. Taylor, C.A.; Fonte, T.A.; Min, J.K. Computational fluid dynamics applied to cardiac computed tomography for non-invasive quantification of fractional flow reserve. *J. Am. Coll. Cardiol.* **2013**, *61*, 2233–2241. [[CrossRef](#)] [[PubMed](#)]
16. Roy, D.; Mazumder, O.; Sinha, A.; Khandelwal, S. Multimodal cardiovascular model for hemodynamic analysis: Simulation study on mitral valve disorders. *PLoS ONE* **2021**, *16*, e0247921.
17. Pironet, A.; Dauby, P.C.; Paeme, S.; Kosta, S.; Chase, J.G.; Desai, T. Simulation of Left Atrial Function Using a Multi-Scale Model of the Cardiovascular System. *PLoS ONE* **2013**, *8*, e65146.
18. Su, B.; Wang, X.; Kabinejadianc, F.; China, C.; Le, T.T.; Zhanga, J.-M. Effects of left atrium on intraventricular flow in numerical simulations. *Comput. Biol.* **2019**, *106*, 46–53. [[CrossRef](#)]
19. Lemmon, J.D.; Yoganathan, A.P. Computational modeling of left heart diastolic function: Examination of ventricular dysfunction. *J. Biomech. Eng.* **2000**, *122*, 297–303. [[CrossRef](#)]
20. Lau, K.; Díaz-Zuccarini, V.; Scambler, P.; Burriesci, C. Fluid–structure interaction study of the edge-to-edge repair technique on the mitral valve. *J. Biomech.* **2011**, *44*, 2409–2417. [[CrossRef](#)]
21. Arts, T.; Delhaas, T.; Bovendeerd, P.; Verbeek, X.; Prinzen, F.W. Adaptation to mechanical load determines shape and properties of heart and circulation: The CircAdapt model. *Am. J. Phys.—Heart Circ. Phys.* **2005**, *288*, H1943–H1954. [[CrossRef](#)]
22. Healy, S.N.; McCulloch, A.D. An ionic model of stretch-activated and stretch-modulated currents in rabbit ventricular myocytes. *Europace* **2006**, *2*, 128–134. [[CrossRef](#)] [[PubMed](#)]
23. Riemer, T.L.; Sobie, E.A.; Tung, L. Stretch-induced changes in arrhythmogenesis and excitability in experimentally based heart cell models. *Am. J. Physiol.* **1998**, *275*, 431–442. [[CrossRef](#)]
24. Vikulova, N.A.; Katsnelson, L.B.; Kursanov, A.G.; Solovyova, O.; Markhasin, V.S. Mechano-electric feedback in one-dimensional model of myocardium. *J. Math. Biol.* **2016**, *2*, 335–366. [[CrossRef](#)] [[PubMed](#)]
25. Li, W.; Kohl, P.; Trayanova, N. Induction of ventricular arrhythmias following mechanical impact: A simulation study in 3D. *J. Mol. Histol.* **2004**, *35*, 679–686. [[CrossRef](#)]
26. Li, W.; Kohl, P.; Trayanova, N. Myocardial ischemia lowers precordial thump efficacy: An inquiry into mechanisms using three-dimensional simulations. *Heart Rhythm* **2006**, *3*, 179–186. [[CrossRef](#)] [[PubMed](#)]
27. Franzone, C.; Pavarino, L.F.; Scacchiet, S. Effects of mechanical feedback on the stability of cardiac scroll waves: A bidomain electro-mechanical simulation study. *Chaos* **2017**, *27*, 093905. [[CrossRef](#)]
28. Kim, E.; Capoccia, M. Synergistic model of cardiac function with a heart assist device. *Bioengineering* **2019**, *7*, 1. [[CrossRef](#)]
29. Hoit, B.D.; Shao, Y.; Gabel, M.; Walsh, R.A. In vivo assessment of left atrial contractile performance in normal and pathological conditions using a time-varying elastance model. *Circulation* **1994**, 1829–1838. [[CrossRef](#)]
30. Suga, H.; Sagawa, K. Instantaneous pressure-volume relationships and their ratio in the excised, supported canine left ventricle. *Circ. Res.* **1974**, *35*, 117–126. [[CrossRef](#)]
31. Claessens, T.E.; Georgakopoulos, D.; Afanasyeva, M.; Vermeersch, S.J.; Millar, H.D.; Stergiopoulos, N.; Westerhof, N.; Verdonck, P.R.; Segers, P. Nonlinear isochrones in murine left ventricular pressure-volume loops: How well does the time-varying elastance concept hold? *Am. J. Physiol. Heart Circ. Physiol.* **2006**, *290*, H1474–H1483. [[CrossRef](#)]
32. Kim, E.; Capoccia, M. Mechano-electric effect and a heart assist device in the synergistic model of cardiac function. *Math. Biosci. Eng.* **2020**, *17*, 5212–5233. [[CrossRef](#)] [[PubMed](#)]
33. Pearce, N.; Kim, E. Modelling the cardiac response to a mechanical stimulation using a low-order model of the heart. *Math. Biosci. Eng.* **2021**, *18*, 4871–4893. [[CrossRef](#)]
34. Tse, G.; Wong, S.T.; Tse, V.; Lee, Y.T.; Lin, H.Y.; Yeo, J.M. Cardiac dynamics: Alternans and arrhythmogenesis. *J. Arrhythm* **2016**, *32*, 411–417. [[CrossRef](#)] [[PubMed](#)]
35. Collet, A.; Bragard, J.; Dauby, P.C. Temperature, geometry, and bifurcations in the numerical modeling of the cardiac mechano-electric feedback. *Chaos Interdiscip. J. Nonlinear Sci.* **2017**, *27*, 093924. [[CrossRef](#)] [[PubMed](#)]
36. Bestel, J. *Modele Differentiel de la Contraction Musculaire Controlee: Application au Systeme Cardio-Vasculaire*. Ph.D Thesis, Universit Paris 9, Paris, France, 2000.
37. Bestel, J.; Clément, F.; Sorine, M. A biomechanical model of muscle contraction. In *Medical Image Computing and Computer-Assisted Intervention MICCAI 2001*; Springer: Berlin, Germany, 2001; pp. 1159–1161.
38. Krejci, P.; Marie, J.; Sorine, M.; Urquiza, J.M. Modelling and Simulation of an Active Fibre for Cardiac Muscle. 2006. Available online: <http://www.crm.umontreal.ca/pub/Rapports/3200-3299/3208.pdf> (accessed on 28 May 2022).
39. Simman, M.A. Rotary Heart Assist Devices. In *Handbook of Automation*; Springer: Berlin/Heidelberg, Germany, 2009; Volume 79, pp. 1409–1422.
40. Lancellott, P.; Marwick, T.; Pierard, L.A. How to manage ischaemic mitral regurgitation. *Heart* **2008**, *94*, 1497–1502. [[CrossRef](#)] [[PubMed](#)]

41. Gaemperli, O.; Biaggi, P.; Gugelmann, R.; Osranek, M.; Schreuder, J.J.; Bühler, I.; Sürder, D.; Lüscher, T.F.; Felix, C.; Bettex, D.; et al. Real-Time Left Ventricular Pressure-Volume Loops during Percutaneous Mitral Valve Repair with the MitraClip System. *Circulation* **2013**, *127*, 1018–1027. [[CrossRef](#)] [[PubMed](#)]
42. Broome, M.; Maksuti, E.; Bjallmark, A.; Frenckner, B.; Janerot-Sjöberg, B. Closed-loop real-time simulation model of hemodynamics and oxygen transport in the cardiovascular system. *Biomed. Eng.* **2013**, *12*, 69. [[CrossRef](#)]
43. Bastos, M.B.; Burkhoff, D.; Maly, J.; Daemen, J.; den Uil, C.A.; Ameloot, K.; Lenzen, M.; Mahfoud, F.; Zijlstra, F.; Schreuder, J.J.; et al. Invasive left ventricle pressure–volume analysis: Overview and practical clinical implications. *Eur. Heart J.* **2020**, *41*, 1286–1297. [[CrossRef](#)]
44. Korakianitis, T.; Shi, Y. Numerical simulation of cardiovascular dynamics with healthy and diseased hearts. *J. Biomech.* **2006**, *39*, 1964–1982. [[CrossRef](#)]
45. Quinn, T.A.; Kohl, P. Cardiac Mechano-Electric Coupling: Acute Effects of Mechanical Stimulation on Heart Rate and Rhythm. *Physiol Rev.* **2021**, *101*, 37–92. [[CrossRef](#)]
46. Coronel, R.; Langerveld, J.; Boersma, L.V.; Wever, E.F.; Bon, L.; van Dessel, P.F.; Linnenbank, A.C.; van Gilst, W.H.; Ernst, S.M.; Opthof, T.; et al. Left atrial pressure reduction for mitral stenosis reverses left atrial direction-dependent conduction abnormalities. *Cardiovasc. Res.* **2010**, *85*, 711–718. [[CrossRef](#)] [[PubMed](#)]
47. Kim, S.; Kuroda, T.; Nishinaga, M.; Yamasawa, M.; Watanabe, S.; Mitsuhashi, T.; Ueda, S.; Shimada, K. Relation between severity of mitral regurgitation and prognosis of mitral valve prolapse: Echocardiographic follow-up study. *Am. Heart J.* **1996**, *132*, 348–355. [[CrossRef](#)]
48. Marks, A.R.; Choong, C.Y.; Sanfilippo, A.J.; Ferré, M.; Weyman, A.E. Identification of high-risk and low-risk subgroups of patients with mitral-valve prolapse. *N. Engl. J. Med.* **1989**, *320*, 1031–1036. [[CrossRef](#)] [[PubMed](#)]
49. Chen, H.Y. Relationship of heart rate turbulence, heart rate variability and the number of ventricular premature beats in patients with mitral valve prolapse and non-significant regurgitation. *Int. J. Cardiol.* **2009**, *135*, 269–271. [[CrossRef](#)]